THE GREAT WORLD OF NANOTECHNOLOGY

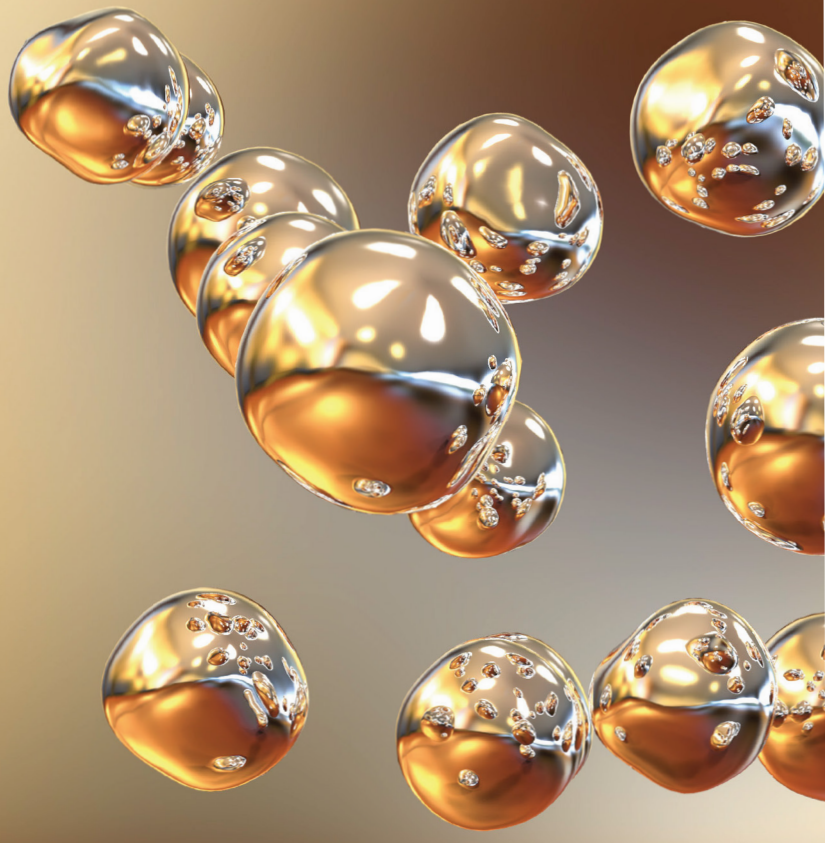

Marcos Augusto de Lima Nobre

(Organizador)

VOL II

EDITORA ARTEMIS
2021

THE GREAT WORLD OF NANOTECHNOLOGY

Marcos Augusto de Lima Nobre

(Organizador)

VOL II

EDITORA ARTEMIS
2021

Editora Chefe Profª Drª Antonella Carvalho de Oliveira
Editora Executiva M.ª Viviane Carvalho Mocellin
Direção de Arte M.ª Bruna Bejarano
Diagramação Elisangela Abreu
Organizadoras Prof. Dr. Marcos Augusto de Lima Nobre
Imagem da Capa Kateryna Kon
Bibliotecário Maurício Amormino Júnior – CRB6/2422

Editora Artemis
Curitiba-PR Brasil
www.editoraartemis.com.br
e-mail:publicar@editoraartemis.com.br

Dados Internacionais de Catalogação na Publicação (CIP)
(eDOC BRASIL, Belo Horizonte/MG)

G786 The great world of nanotechnology [livro eletrônico] : vol. II /
Organizador Marcos Augusto de Lima Nobre. – Curitiba, PR: Artemis, 2021.

Formato: PDF
Requisitos de sistema: Adobe Acrobat Reader
Modo de acesso: World Wide Web
Inclui bibliografia
Edição bilíngue
ISBN 978-65-87396-36-1
DOI 10.37572/EdArt_300621361

1. Nanociência. 2. Nanotecnologia. I. Nobre, Marcos Augusto Lima.

CDD 620.5

Elaborado por Maurício Amormino Júnior – CRB6/2422

EDITORA ARTEMIS
2021

Editora Artemis
Curitiba-PR Brasil
www.editoraartemis.com.br
e-mail:publicar@editoraartemis.com.br

PREFACE

The insertion of new and enhanced materials based on materials belonging to the Nano scale in the day-by-day has growth up in a silent way. In part, a number of works in the nanotechnology stemming of theoretical research using Density Functional Theory (DFT) and sophisticated simulation methods; another part is associated to the protected technologies associated to the military and patented nanomaterial and its process. In this sense, open access to recent aspects on the nanostructures application and properties can be reached in this book. Here, an interesting set of chapters gives opportunity of access texts that reach process and processing of nanostructures, applications of nanotechnology, advanced techniques to theoretical development. A broad set of nanostructures are here covered such as, nanocrystal, superficial nanograins, inner microstructures with nanograins, nanoaggregates, nanoshells, nanotubes, nanoflowers, nanoroad, nanosheets, Also, reveals new investigations areas as grainboundary of nanograins in ceramics and metals. A great number of software has been used as a tool of development of Science and Technologies for nanotechnology COMSOL Multiphysics 5.2. Phenomena and properties has been investigated by recent or classical techniques of materials characterization as Localized Surface Plasmon Resonance (LSPR), X-ray photoelectron spectroscopy (XPS), Field Emission Gun Scanning Electron Microscopy (FEG-SEM) with Energy Dispersive Spectroscopy (EDS), Raman Scattering Spectroscopy (RSS), X ray diffraction (XRD), ^{57}Fe Mössbauer spectroscopy, UV-vis spectroscopy, dynamic light scattering (DLS), Atomic Force Microscopy (AFM), and Field Emission Gun Scanning Electron Microscopy (FEG-SEM). In this sense, collections of spectra from Mössbauer spectroscopy, UV-vis spectroscopy and Infrared spectroscopy can be found. As a matter of fact, some chapter's item can be seemed as specific protocols for synthesis, preparations and measurements in the nanotechnology.

I hope you enjoy your reading.

Prof. Dr. Marcos Augusto Lima Nobre

TABLE OF CONTENTS

CHAPTER 8

X-RAY PHOTOELECTRON SPECTROSCOPY (XPS) STUDY OF CONDUCTIVE TUBE AFTER NITROGEN PIII

Data de submissão: 29/03/2021
Data de aceite: 22/04/2021

Pericles Lopes Sant'Ana
São Paulo State University (UNESP)
Technological Plasmas Laboratory
Sorocaba, SP, Brazil
drsantanapl@gmail.com
http://lattes.cnpq.br/3752107640196845

Nazir Monteiro dos Santos
National Institute for Space Research
Associated Laboratory of Plasma
São José dos Campos, SP, Brazil
nazirmonteiro@gmail.com
https://orcid.org/0000-0002-1518-9403

Elver Juan de Dios Mitma Pillaca
National Institute for Space Research
Associated Laboratory of Plasma
São José dos Campos, SP, Brazil
elver.mitma@inpe.br
https://orcid.org/0000-0003-4893-8893

Mario Ueda
National Institute for Space Research
Associated Laboratory of Plasma
São José dos Campos, SP, Brazil
mario.ueda@inpe.br
http://lattes.cnpq.br/9226460532838417

Steven Frederick Durrant
São Paulo State University (UNESP)
Technological Plasmas Laboratory
Sorocaba, SP, Brazil
steven.durrant@unesp.br
https://orcid.org/0000-0002-4511-3768

ABSTRACT: This work reports an X-ray photoelectron spectroscopy (XPS) study of inner surface modification of stainless steel (SS) conducting tubes after nitrogen plasma immersion ion implantation (PIII) within a non-uniform magnetic field. Nitrogen PIII was carried out in tubes of length 150 mm and diameters (D) of 110 mm, 40 mm and 15 mm, for two arrangements: (a) a tube with an auxiliary electrode (AE) and (b) a tube without an AE. Metal nitrides (CrN, Cr_2N and FeN) and oxide states were observed by XPS in all cases. In the presence of an AE, however, a significant reduction in oxidation and an increase in Cr_2N for the tube with D = 40 mm were detected. Consequently, the wear rate decreased by about a factor of ten compared with the case without an AE.
KEYWORDS: Chemical composition of SS surface. Plasma immersion ion implantation. X-ray photoelectron spectroscopy. PIII in magnetic field.

1 INTRODUCTION

Plasma immersion ion implantation (PIII) is a widely used technique for the

surface modification of materials, employed mainly to improve mechanical, chemical, and tribological properties of complex-shaped three-dimensional objects [1]. To alter a material's surface properties, however, the treatment must achieve a high dose and conformal coverage [2]. These issues were discussed in several investigations, where it was suggested that the dose obtained could be influenced by the target geometries [3] [4]. Effective implantation is difficult in workpieces with concave, rather than flat or convex, geometry [5]. An example where PIII is ineffective is within metallic tubes, which are extensively used in the industry. According to Sheridan [4][6], this problem is caused by low ion energy during PIII. Possibly, this is caused by the reduction of the electric potential inside the tube, which is related to the aspect ratios: (a) the ratio between the tube radius and their length (R/L) [5] [7]; (b) ratio between the tube radius and the overload radius (R/D) [6] [8]. This approach is important because depending on the radius, the dose can be maximized producing a large number of ions with high impact energy bombarding the tube inner surface. Electron cyclotron resonance (ECR) and microwave discharges have been proposed in recent decades to produce greater doses, especially in small diameter tubes [9, 10].

Recently, PIII has been extensively used to improve some properties of austenitic stainless steel tubes. Stainless steel offers high corrosion resistance, low wear resistance and reduced hardness. These properties can be improved if implantation of nitrogen with a high retained dose is performed. To satisfy this condition requires a minimum temperature (of 350 to 400 °C) in the tube to activate the diffusion process. Nitrogen diffusion caused by the increased temperature during implantation could cause great changes in surface properties owing to the formation of new phases (γ_N) and structures (chromium and iron nitrides). Thus, stainless steel tubes with this new surface layer could enhance significantly their properties. If, however, the temperature exceeds 450 °C, the available chromium for chromium oxide can be reduced and there will be a decrease in the corrosion resistance [11].

Recently, interest has arisen in the possibility of using a magnetic field to enhance the PIII process for the treatment of tubes made of stainless steel [12, 13]. The principal advantage of this approach is related to promoting an electric discharge at low gas pressure [14]. This is possible owing to the presence of a magnetic field transversal to the electric field. In this configuration, a region with high plasma density is created via the intense background gas ionization caused by the trapped electrons where the **E** and **B** fields cross [11, 15]. Additionally, if an earthed electrode is introduced along the axis of the tube, the discharge occurs preferentially within Successful PIII depends on such conditions since higher pressures would cause undesirable arcing [16].

Thus, the major objective of this work is to study the effects of nitrogen implantation on the changes in chemical composition of the inner surfaces of SS 304 tubes, using X-ray photoelectron spectroscopy (XPS), after performing PIII in a non-uniform magnetic field. Special attention is given to the analysis of the Fe 2p, Cr 2p and N 1s regions of the spectra. The analyses are completed with studies employing atomic force microscopy (AFM), scanning electron microscopy (SEM) and wear rate measurements to characterize the inner surfaces of the tubes. Tubes of D = 110 mm, 40 mm and 15 mm were studied in two arrangements: (a) tube with an auxiliary electrode and (b) tube without an auxiliary electrode.

2 EXPERIMENTAL

In this work, tubes made of AISI type 304 Stainless Steel (SS), whose chemical composition is given in **Table I**, were used to perform nitrogen PIII on their inner surfaces.

Table I: Chemical composition (%) of type 304 Stainless Steel (SS) tubes

Iron	*Carbon*	Chrome	Manganese	Silicon	Phosphorus	Sulfur	Nickel	Nitrogen
67 to 72	0.07	18.00	2.00	1.00	0.045	0.015	8.00	0.10

This stainless steel was chosen since it has received considerable attention from the scientific and industrial community, owing to its excellent resistance to corrosion, low cost and extensive use in the manufacturing industry. Nitrogen ion implantation was carried out in a vacuum chamber of 20 liters with a system of two magnetic coils mounted on it to produce a non-uniform magnetic field configuration (magnetic bottle). This system is described in detail elsewhere [14]. Inside the chamber, metallic tubes of length 150 mm and diameters of 110 mm, 40 mm and 15 mm were placed on the axis to coincide with the region where the magnetic field has its minimum value. A SS grounding rod, 2 mm in diameter, was placed inside each tube to work as an auxiliary electrode (AE). For characterization of the inner surface of the tubes, specimens made of SS 304 (3 mm thickness and 7.5 mm radius) were prepared. Five SS sample equidistantly distributed along the 150 mm length were used in each tube. The tubes were polished and subsequently cleaned in an ultrasound bath just before their insertion into the tubes with diameters of 110 mm and 40 mm. For the tube of smallest diameter (15 mm), five holes (diameter of 8 mm) were perforated equidistantly along the surface, to expose them to the internal plasma. A system of mechanical and diffusion pumps was used to reduce the pressure to about 2.0×10^{-2} Pa. Later, nitrogen gas was admitted into the system, reaching a working pressure of 3 Pa. The PIII treatment conditions were kept constant throughout the experiment, with 20 μs pulses of 6 kV at 500 Hz. The total current on the

target was measured with a Rogowski coil installed in the high voltage pulser. An infrared thermometer Micron model M90 with range between 250 - 2000 °C was used to monitor the temperature of the tubes. Measurements of total current density (*j*) and temperature (T) during the treatment of tubes for large, medium and small diameters are shown in **Table II**. Finally, the tubes were PIII treated for 60 min in a non-uniform magnetic field with an intensity between 60 G and 90G.

Table II: Current density (*j*) and temperature (T) for tubes with D = 110 mm, D = 40 mm and D = 15 mm after 60 min. of treatment with and without AE and in presence of magnetic field.

	D =110 mm		D = 40 mm		D = 15 mm
	Without AE	With AE	Without AE	With AE	Without AE
j (mA/cm²)	7.33	7.72	10.6	15.9	28.3
T (°C)	< 250	< 250	340	475	440

After the treatment, samples placed on the inner surface of the tubes were characterized. Only the SS sample placed in the center part of each tube was used for all the characterization tests. Chemical composition was measured using XPS on a Kratos Axis Ultra^{DLD} electron spectrometer. The experimental resolution of the binding energy was less than 0.5 eV. Samples were excited with monochromatic Al κ_{α} radiation (1486.6 eV) in an ultra-high vacuum of pressure less than 10^{-7} Pa, an acceleration voltage of 15 kV and a current of 10 mA. After Shirley-type background correction [15], peak fitting was performed using the Casa XPS software (2.3.15 version) with mixed Gaussian/Lorentzian (70/30) functions and least-squares fitting [16]. The chemical state of the SS sample after treatment was tested by examining the spectra of the Fe 2p and Cr 2p and N 1s regions after argon ion sputtering for 600 s.

For XPS depth profiling of samples (tubes of D = 110 mm and 40 mm) treated by NPIII, the analysis area was 110 μm × 110 μm (small spot mode) for 600 s, resulting in a sputter rate of 10 nm/min. In the untreated sample and the treated inner tube of D=15mm, the analysis were only superficial, the sputtering of an area of 700 x 300 μm (large spot mode) for 600 s was performed with an Ar^+ ion gun (4 keV), resulting in a sputter rate of 0.2 nm/min.

The assessment of the wear damage was performed with a microscope and a profilometer, following a pin-on-disk test in a CSM-Instruments tribometer. This was operated with a load of 1.0 N in air at a relative average humidity of about 47 %. An alumina ball of 3.0 mm diameter with fixed linear velocity of 5 cm/s was used. A NanoScope V microscope, operated in the tapping mode, was used to analyze surface topography and roughness (R_q)

over a scanning area of 15 µm x 15 µm. Wear width was observed by SEM using an electron beam of 20.0 keV at a magnification of 500x, and a scanning time of 100 s.

3 RESULTS AND DISCUSSIONS

3.1 ELEMENTAL COMPOSITION

As XPS is a surface analysis technique, depth profiling of the samples was obtained by combining a sequence of ion gun etch cycles interleaved with XPS measurements. An ion gun was used to etch the material for 600 s before being turned off while XPS spectra were acquired. Each ion gun etch cycle exposed a new surface and the XPS spectra allowed determination of the composition of the exposed surfaces. Elemental concentrations were thus revealed as a function of etch-time.

Figure 1 shows XPS elemental concentrations seen after ion implantation for tubes with D = 110 mm: (a) without AE and (b) with AE; for tubes with D = 40 mm: (c) without AE and (d) with AE (e) D15 without AE (f) SS 304 untreated.

Fig. 1(a, b) shows XPS concentration profiles of O, Fe, C, Cr, Mn, Ni and N elements present for the tube with D = 110 mm. In the absence of an AE, [N] on the surface began at 2.5 at %, increasing to 5 at % and remaining constant thereafter. When an AE was introduced into the tube, [N] roughly doubled, then fell to about 5 at % at 180 s. The [Ni] was negligible until 420 s of etching (Fig. 1(a)). With an AE [Ni] initially rises, and reaches a plateau at ~150 s. Both with and without an AE, a significant [Mn] appears only at ~400 s.

For the tube with D = 40 mm without AE, as shown in Fig. 1(c), [N] was initially zero and increased monotonically, reaching 5 at % at the end of the test. Similarly, a low [Cr], close to zero, may be observed. The C composition shows high atomic concentration (70 at %) on the surface and then falls, to reach ~8 at.% after 600 s. As can be seen in Fig. 1(d), when an AE is introduced, [Cr] and [N] increase throughout the etching process. Furthermore, no Mn or Ni was detected while [C] is similar to that found in the tube with D = 110 mm with and without the use of an AE. Both [Fe] and [O] profiles show plateaus throughout the argon ion sputtering. These results are similar to that for the tube with D = 15 mm (figure not shown) where a low [N] and [Cr] of about 1.5 at % were detected. For both tubes (D = 40 mm and D = 15 mm) there were plateaus of high [Fe] and [O]. This suggests the formation of an oxide layer on the surface, even though the same conditions were used for all cases. These facts can be attributed to a rise in temperature caused by the reduction in tube diameter, as suggested by the temperature measurements shown in **Table II**.

Fig. 1: XPS elemental compositions seen after ion implantation for tubes with D = 110 mm: (a) without AE and (b) with AE; for tubes with D = 40 mm: (c) without AE and (d) with AE (e) D15 without AE (f) SS 304 untreated.

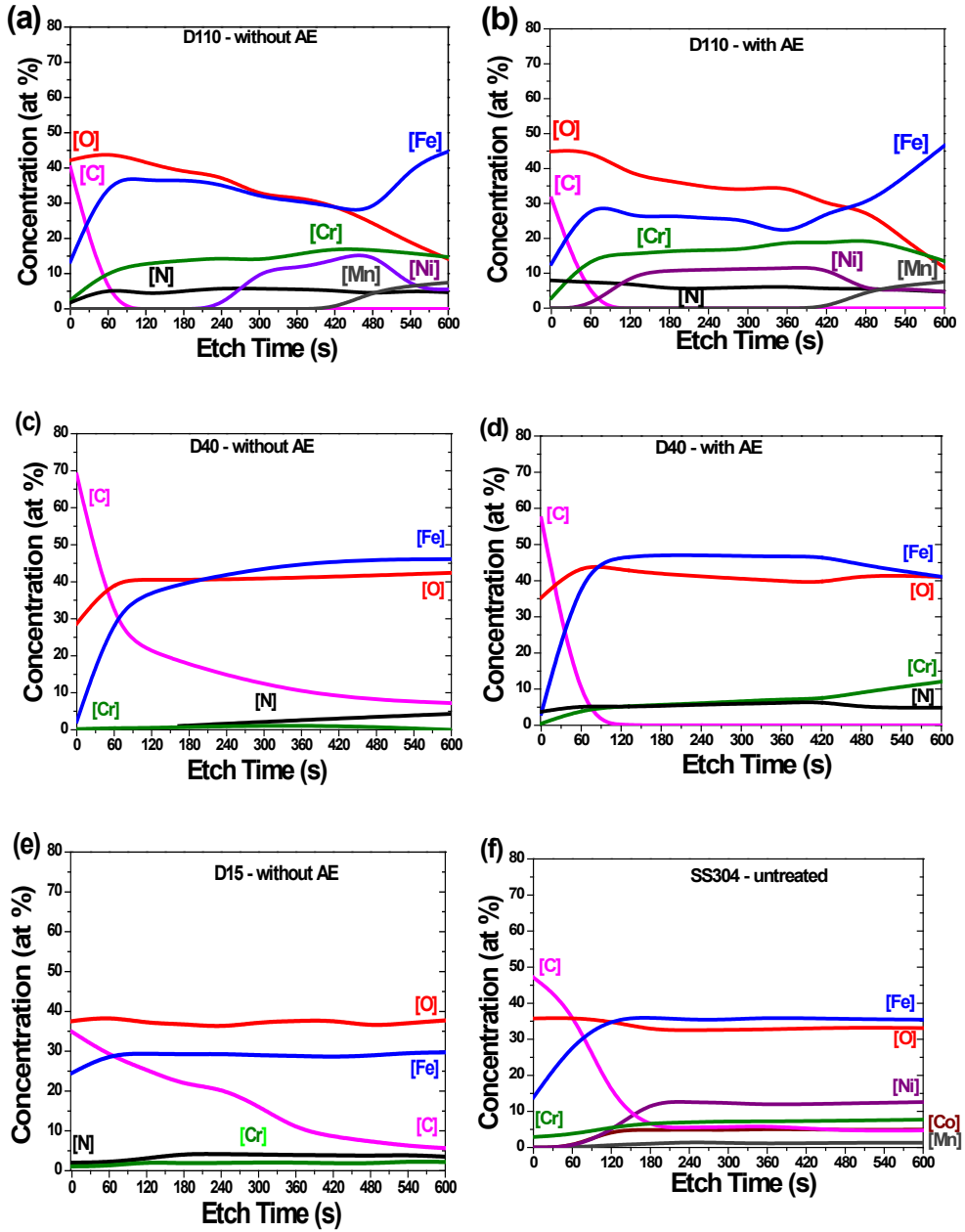

After the elemental concentration profile analysis, the chemical states formed after PIII in tubes with D = 110 mm, 40 mm and 15 mm were investigated. High resolution spectral lines of Fe 2p, Cr 2p, and N 1s regions were considered because they are responsible for the chemical modification of the SS surface. Only XPS spectra for the tube with D = 40

mm are shown in Fig. 2 owing to the high current measured for this case, as can be seen in **Table II**; these are displayed in panels for Cr 2p and N 1s regions. However, information concerning binding energy, chemical state, atomic concentration and author references for Fe $2p_{3/2}$, Cr $2p_{3/2}$ and N 1s spectral lines in tubes with D = 110 mm and D = 15 mm are listed in Table **III**, for the SS304 untreated and treated samples [17-23].

3.2 CR 2P REGION

Fig. 2m (a, b, c, d, e, f) show deconvoluted XPS spectra of the Fe 2p, Cr 2p and N 1s regions for the tube with D = 40 mm, with and without AE.

Fig. 2: Spectra of Fe 2p, Cr 2p and N 1s regions for the tube of D = 40 mm. Without AE: (a), (c) and (e); With AE: (b), (d) and (f).

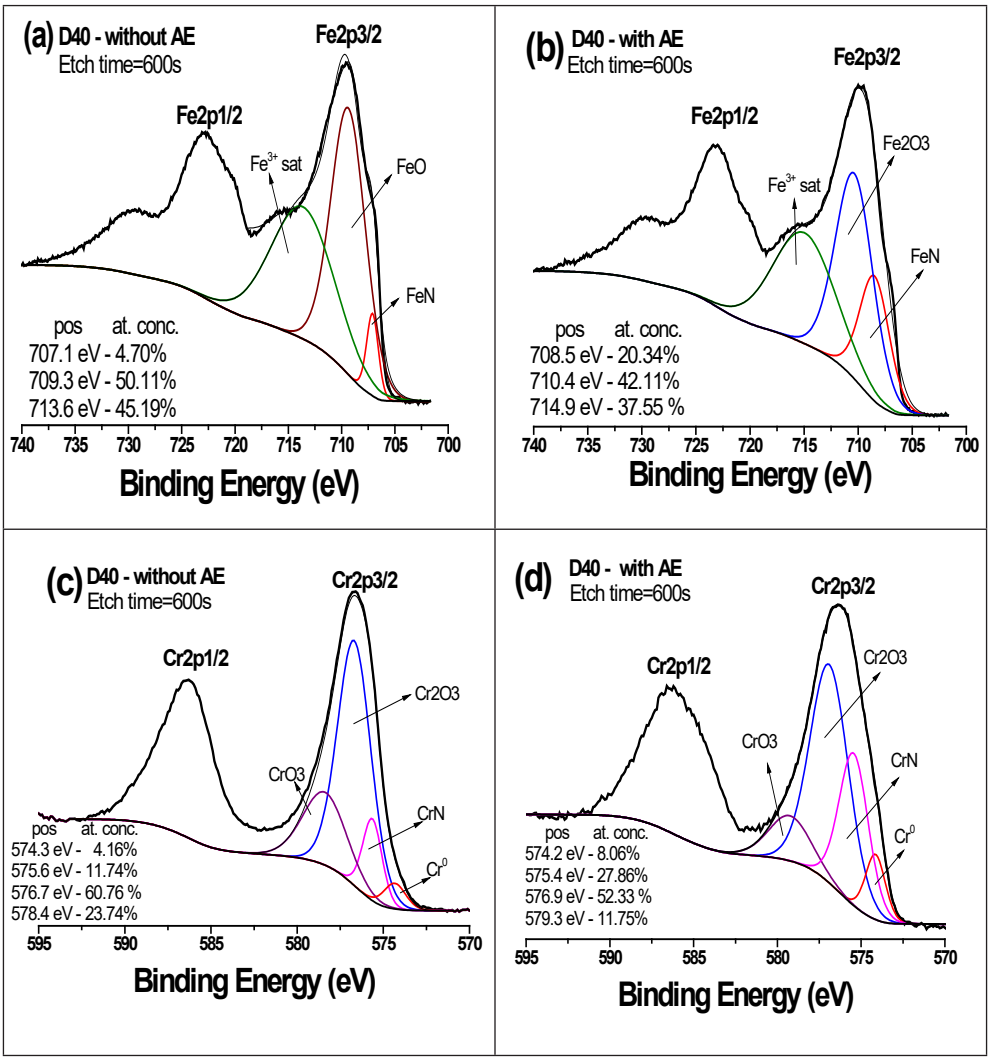

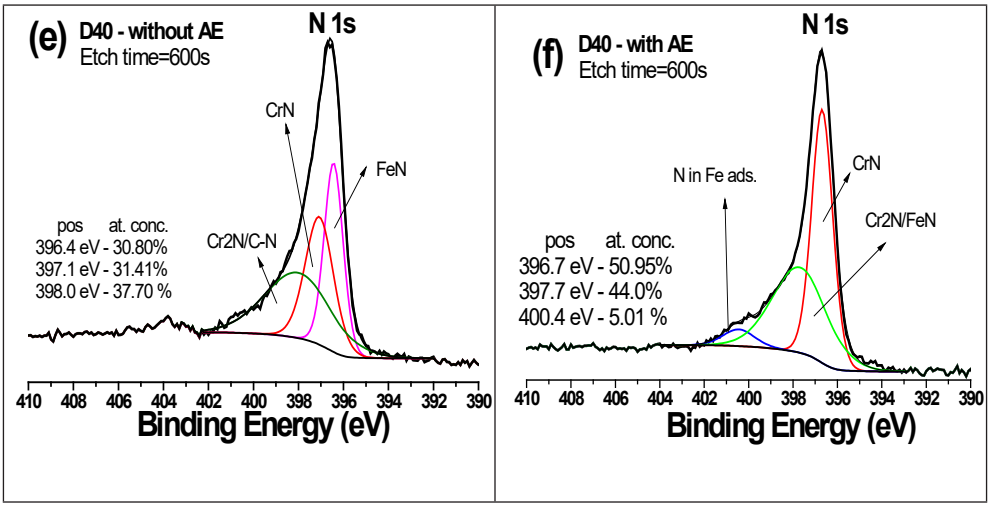

High intensity peaks of chromium-oxide (Cr_2O_3) after PIII are identified. Both CrN and CrO_3 were also found for the both cases. According to the results of **Table III**, there is a decrease in the Cr_2O_3/CrN ratio from 5.2 to 1.9 when an AE is used. This indicates a greater [CrN] in the presence of an AE. For the tube with D = 110 mm, results presented in Table III indicate the presence of Cr_2N peaks with similar intensities when the treatments are performed with and without AE. However, the Cr_2N group was not detected when the diameter of tube was reduced from 110 mm to 40 mm. In the absence of AE, the Cr_2O_3/CrN ratio was 5.2 whereas it decreased to 1.9 when the AE was introduced. This result indicates a greater presence of CrN than Cr_2O_3 which resulted in increased surface hardness [24].

For the tube with D = 15 mm without AE, chromium oxide (Cr_2O_3) and metallic chromium were identified on the treated surface. These results are similar to the untreated sample case. For this diameter of tube, no formation of CrN was detected, even though the temperature in the tube increased to 440 °C (see Table II). It is possible that the low ion energy inside the tube was insufficient to promote this kind of chemical bond or the CrN layer was sputtered away.

3.3 N 1S REGION

The N 1s high resolution fitted spectra for the tube with D = 40 mm treated without an AE is shown in Fig. 2(e) The chemical states in this sample presented FeN (396.4 eV), CrN (397.1 eV) and revealed Cr_2N (398.0 eV). Some authors [20, 21] assign such peak energies (398.0 eV) to C-N. This coincides with the results observed throughout the etching time profile shown in Fig. 1(e), where an appreciable amount of contaminant carbon

remains near the surface after argon ion sputtering. For the case with an AE, evidence of high intensity CrN and Cr_2N and/or FeN peaks was identified in Fig. 2(d). In addition, a weak peak observed at 400.4 eV indicates the possible presence of nitrogen absorbed in the Fe lattice [23]. We assume in this work that [Cr_2N] is significantly greater than [FeN] owing to the high nitrogen ion current measured during the treatment (see Table II). On the other hand, for D = 110 mm, data of binding energies reported in **Table III** indicate the presence of CrN, Cr_2N and/or FeN and nitrogen adsorbed in iron for the cases with and without an AE. With exception of nitrogen adsorbed in iron, similar concentrations at% of Cr_2N and/or FeN and CrN were obtained for both cases.

When the tube diameter was reduced from 110 mm to 40 mm, the XPS results showed a decrease in the Cr_2N/CrN intensity ratio, from 1.8 to 1.2, for the case without an AE, whereas with an AE it decreased from 1.7 to 0.9. These results indicate the presence of greater [CrN] in the tube with D = 40 mm with an AE. Another characteristic is the partial reduction of nitrogen adsorbed in iron for the case with an AE, and its total absence without an AE.

For D = 15 mm, the results shown in Table III indicate the presence of a high intensity peak at 403.4 eV that is related to NO_2. Nitrogen adsorbed into iron was attributed to the peak at 400.1 eV, whereas the presence of FeN was identified at 396.4 eV. No Formation of CrN peak can be resulted to the increase of current density (j) and of the temperature of the PIII.

3.4 FE 2P REGION

Binding energies of the Fe 2p region for the tube with D = 40 mm, with and without AE are reported in Table III. After nitrogen PIII, FeN is detected for both arrangements as well as the satellite iron (Fe^{3+} sat), corresponding to SS304. The oxidation states were modified from FeO to Fe_2O_3, however, after introduction of the AE. However, the FeO/FeN to Fe_2O_3/FeN intensity ratio fell from 10.7 to 2.07. This indicates larger presence of FeN which was favored perhaps by higher temperatures during PIII.

On the other hand, information shown in **Table III** for the tube with D = 110 mm, without an AE, revealed bonding energies corresponding to FeN. Metallic iron (α-Fe) in the ground state, and Fe_2O_3 corresponding to iron oxide present in the bulk were also identified. After introduction of AE in PIII, similar chemical states were obtained, which indicate no significant changes with respect to these states.

Remarkable differences are observed when the tube diameter is reduced from 110 mm to 40 mm. For D = 40 mm, changes of oxidation states from Fe_2O_3 to FeO are

found for the tube without an AE. Perhaps, this is caused by the increase in temperature promoted by the high ion flux bombarding the surface (see current in Table II) which was favorable to oxidation. Another significant change detected is the variation of Fe_2O_3/FeN ratio. The analysis for the case with AE indicated an increment from 1.9 to 2.07. As can be noticed from this result, this occurs only when an AE is introduced into the tube.

Results obtained for D = 15 mm without an AE are compared to those of the untreated sample because it was not possible to perform an experiment with an AE in this case (the tube diameter was too small). As can be seen from Table III, the atomic concentration of the Fe_2O_3 oxidation state increased and a new FeO oxidation stage appeared after PIII. Although a high current density was measured, no FeN was observed, as indicated by the data shown in Table II.

In summary, iron oxide was present in all the analyzed tubes. This is attributed to the high affinity between oxygen and iron, which is favored by higher temperatures. Looking at Table II, a dependence on temperature is seen as the tube diameter is reduced (110 mm to 15 mm). The temperature increase is caused by ion implantation. This is consistent with the results shown in Fig. 1(a), which suggests thicker oxygenated layers after 600 s etching. The cause of so much oxygen, however, is not yet clear. Possibly, the intense electric field created at the ends of the tubes, promotes greater ionization of the gas. Clearly, the specific distribution of the magnetic field is also a contributing factor. Implanted oxygen may also originate from residual and adsorbed gas and water vapor.

Table III: Results of the XPS analyses. Binding Energy, chemical state and atomic concentration of standard and samples treated by nitrogen PIII for tubes with D = 110 mm, D = 40 mm and D = 15 mm.

Samples	**Fe $2p_{3/2}$**				**Cr $2p_{3/2}$**				**N 1s**			
	BE (eV)	Chemical state	*at%	Ref	BE (eV)	Chemical state	*at%	Ref	BE (eV)	Chemical state	*at%	Ref
SS304 untreated	706.9	Fe^{o}	1.8	[22]	574.1	Cr^{o}	4.4	[22]				
	709.9	FeO	34.7	[23]	576.6	Cr_2O_3	95.6	[22]				
	714.9	Fe^{3+} sat	63.5	[25]								
D110 with AE	706.7	Fe^{o}	21.9	[22]	573.9	Cr^{o}	13.1	[22]	396.9	CrN	30.4	[22, 24]
	707.7	FeN	27.4	[26, 27]	574.6	CrN	24.6	[22]	397.7	Cr_2N/FeN	50.4	[22]
	710.4	Fe_2O_3	50.7	[22]	576,4	Cr_2N	62.4	[22]	399.9	N ads	19.2	[27]

Samples	Fe $2p_{3/2}$				Cr $2p_{3/2}$				N 1s			
	BE (eV)	Chemical state	*at%	Ref	BE (eV)	Chemical state	*at%	Ref	BE (eV)	Chemical state	*at%	Ref
D110 without AE	706.7	Fe^0	21.5	[22]	573.7	Cr^0	13.7	[22]	396.9	CrN	25.7	[22, 24]
	707.6	FeN	27.0	[26, 27]	574.3	CrN	26.6		397.6	Cr_2N/FeN	47.1	[22]
	710.4	Fe_2O_3	51.5	[22]	576.1	Cr_2N	59.8	[22]	399.2	N ads	27.2	[27]
D40 with AE	708.5	FeN	20.3	[26]	574.2	Cr^0	8.1	[22, 23]	396.7	CrN	50.9	[22, 24]
	710.4	Fe_2O_3	42.1	[22]	575.4	CrN	27.9	[22]	397.7	Cr_2N/FeN	44.0	[22]
	714.9	Fe^{3+} sat	37.6	[25]	576.9	Cr_2O_3	52.3	[22]	400.4	N ads	5.0	[27]
					579.3	CrO_3	11.8	[22, 24]				
D40 without AE	707.1	FeN	4.7	[22]	574.3	Cr^0	4.2	[22]	396.4	FeN	30.8	[26]
	709.3	FeO	50.1	[22, 24]	575.6	CrN	11.7	[22, 23]	397.1	CrN	31.4	[22]
	713.6	Fe^{3+} sat	45.2	[25]	576.7	Cr_2O_3	60.8	[22]	398.0	Cr_2N/C-N	37.7	[25, 26]
					578.4	CrO_3	23.7	[25]				
D15 without AE	709.4	FeO	27.7	[22, 24]	573.9	Cr^0	6.4	[22]	396.4	FeN	27.5	[26]
	711.4	Fe_2O_3	48.3	[22, 24]	576.6	Cr_2O_3	93.6	[22]	400.1	N ads	10.4	[27]
	717.8	Fe^{3+} sat	23.9	[25]					403.4	NO_2	62.2	

*atomic concentration (at%)

3.5 SURFACE MORPHOLOGY AND WEAR RATE

We also examined the topography of the inner surfaces of the tubes and their surface roughness (R_q) using AFM images. AFM images are shown in Fig. 3 and R_q data are reported in **Table IV**.

In Fig. 3(a) an AFM image of the untreated sample is show the scratches caused by the polishing are visible. Fig. 3 (b, c) shows AFM images of samples treated in the tube with D = 40 mm with and without an AE. In Fig. 3(b) for tube with D= 40 mm without an AE, the image is similar in morphology to the untreated one shown in Fig. 3(a). The morphology is similar to that observed in all of the implanted samples, except for the tube with D = 40 mm with an AE. It is possible to see a significant, change in surface morphology after the treatment was performed with the presence of an AE.

Fig. 3: AFM images of untreated tube (a), D = 40 mm without an AE (b), D = 110 mm with an AE (c).

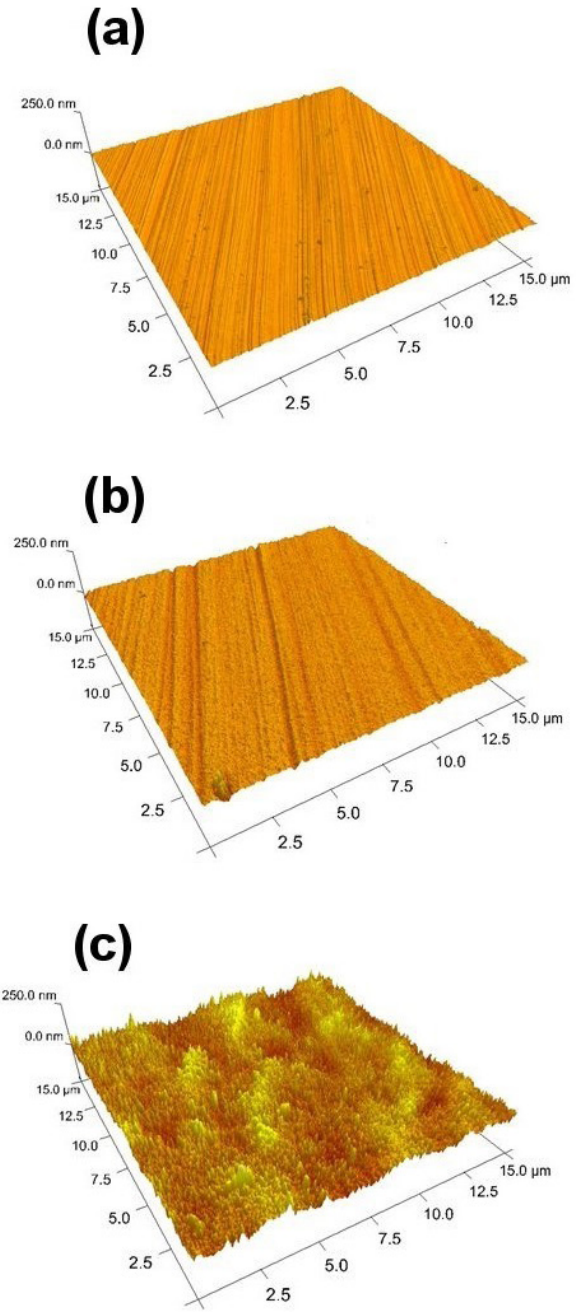

The selection of this AFM image as representative was based on the similar R_q values reported in Table IV which indicate a small increase from 3.6 nm (untreated tube) to 4.0 nm for tube with D= 40 mm, and 6.8 nm for tube with D = 15 mm of treatment without AE. When an AE was introduced into the tube with D = 40 mm, however, the AFM image in

Fig 3(c) revealed strong erosion of the sample surface, producing an increase in R_q, from 4.0 nm to 14 nm. This result can be attributed to a greater ion current (about16 mA/cm^2) and temperature (475 °C), how can be seen in the Table II, causing higher sputtering rate and higher ion flux hitting the tube inside wall.

Table IV: Roughness and wear rates for tubes with D = 110 mm, D = 40 mm and D = 15 mm after 60 min of treatment with and without AE.

	D =110 mm		D = 40 mm		D= 15 mm
	Without AE	With AE	Without AE	With AE	Without AE
Roughness (nm)	-	5.3	4.0	14.0	6.8
Wear (x10^{-5} mm^3/Nm)	19.0	4.0	6.0	0.6	3.0

Wear results reveal a significant reduction of 19 x10^{-5} mm^3/Nm to 4 x10^{-5} mm^3/Nm for samples treated in discharge with the presence of the AE, for D=40 mm tube. For D=110 mm tube when the AE was not used, the value of wear was from 6 x10^{-5} mm^3/Nm and reduced to 0.6 x10^{-5} mm^3/Nm with the presence of AE. This can be explained by the XPS results discussed in 3.2 section where the increase of bonded Cr_2N on the surface favored a decrease in wear. This did not happen for D = 110 mm without an AE, where a high wear rate was measured (19 x 10^{-5} mm^3/Nm), however, as listed in Table IV. Typical widths of wear tracks caused by the ball of a pin-on-disk system are seen in the SEM images of Fig. 4. One possible explanation for this result may be deduced from the etch time profiles of Fig 1(a, b), where the surface Ni concentrations are different. Recent studies [25] have associated that result with surface oxidation rather than nitrogen implantation/diffusion. Another investigation showed the presence of residual oxygen gas, depending on the gas feeding system in PIII experiments, which contributes to the copious formation of oxides [26].

Fig. 4: Images of the wear caused by the ball of a pin-on-disk system seen by scanning electron micrography of untreated tube (a), D = 40 mm tube without an AE (b), D = 40 mm tube with an AE (c).

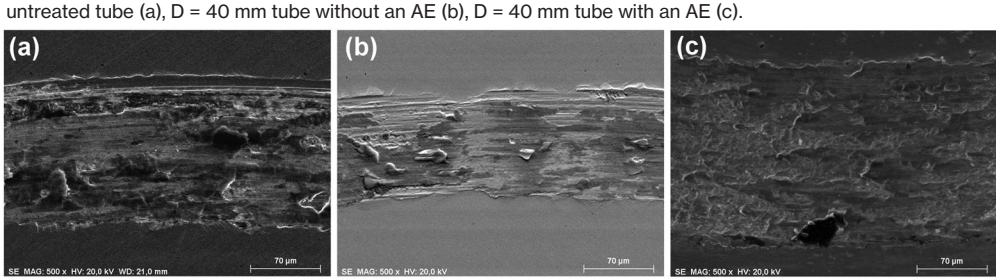

4 CONCLUSIONS

Effects of nitrogen ion implantation on the inner walls of tubes as a function of their diameters were studied by XPS, after performing PIII employing a magnetic field using two

arrangements: SS tubes with and without AE. The Fe 2p, Cr 2p and N1s regions of the XPS spectra were used to study the chemical state of SS specimens. A dependence of the nitrogen incorporation on the tube diameter was revealed. This was most evident in a tube with D = 40 mm and in the presence of an AE, where the ion bombardment of the surface was intense. A surface with CrN, Cr_2N and FeN of high roughness was detected. As a consequence, the resistance against wear was improved about five times compared to the one without an AE. In the other cases (tubes with D = 110 mm with an AE and D = 15 mm without AE), the wear rate and surface topography were similar to the untreated sample. Finally, the presence of a high concentration of oxide on the top surface, in all tubes, was detected by XS after PIII. The effect increased for the tube smaller diameters. We conclude that PIII treatments inside the tubes were enhanced by the presence of the magnetic field for all three size tubes. It was particularly favorable for the case with the introduction of an AE for medium diameter (D = 40 mm) one.

5 ACKNOWLEDGMENTS

This work was supported by the São Paulo State Research Foundation (FAPESP, 15/09781-0), the National Council for Scientific and Technological Development (CNPq), and the Ministry of Science Technology and Innovation (MSTI). This study was also financed in part by Coordination for the Improvement of Higher Education Personnel – Brazil (CAPES).

REFERENCE

[1] A. Anders, Handbook of Plasma Immersion Ion Implantation and Deposition, Jhon Wiley & Sons, Inc, 2000.

[2] D.J. Rej, R.J. Faehl, J.N. Matossian, Key issues in plasma-source ion implantation, Surf. Coatings Technol. 96 (1997) 45–51. doi:10.1016/S0257-8972(97)00095-9.

[3] T.E. Sheridan, J.A. Goree, Analytic expression for the electric potential in the plasma sheath, IEEE Trans. Plasma Sci. 17 (1989) 884–888. doi:10.1109/27.41228.

[4] T.E. Sheridan, Analytic theory of sheath expansion into a cylindrical bore, Phys. Plasmas. 3 (1996) 3507. doi:10.1063/1.871501.

[5] B. Liu, G. Zhang, D. Cheng, C. Liu, R. He, S.-Z. Yang, Inner surface coating of TiN by the grid-enhanced plasma source ion implantation technique, J. Vac. Sci. Technol. A Vacuum, Surfaces, Film. 19 (2001) 2958. doi:10.1116/1.1415356.

[6] E. J D. M. Pillaca; M. Ueda; S. F. M. Mariano, R. O. Moraes. Reprint of Study of plasma immersion ion implantation inside a conducting tube using an E x B field configuration. Surface & Coatings Technology, 256 (2014) 73–77.

[7] C.B. Mello, M. Ueda, C.M. Lepienski, H. Reuther, Tribological changes on SS304 stainless steel induced by nitrogen plasma immersion ion implantation with and without auxiliary heating, Appl. Surf. Sci. 256 (2009) 1461–1465. doi:10.1016/j.apsusc.2009.09.001.

[8] X.B. Tian, Y.X. Leng, T.K. Kwok, L.P. Wang, B.Y. Tang, P.K. Chu, Hybrid elevated-temperature, low/high-voltage plasma immersion ion implantation of AISI304 stainless steel, Surf. Coatings Technol. 135 (2001) 178–183. doi:10.1016/S0257-8972(00)00996-8.

[9] M. Samandi, B.A. Shedden, D.I. Smith, G.A. Collins, R. Hutchings, J. Tendys, Microstructure, corrosion and tribological behaviour of plasma immersion ion-implanted austenitic stainless steel, Surf. Coatings Technol. 59 (1993) 261–266. doi:10.1016/0257-8972(93)90094-5.

[10] E.J.D.M. Pillaca, M. Ueda, H. Reuther, C.M. Lepienski, Study of the effects of plasma immersion ion implantation on austenitic stainless steel using E×B fields, Surf. Coatings Technol. 246 (2014) 1–5. doi:10.1016/j.surfcoat.2014.02.044.

[11] E.J.D.M. Pillaca, M. Ueda, K.G. Kostov, Investigation of Plasma Immersion Ion Implantation Process in Magnetic Mirror Geometry, IEEE Trans. Plasma Sci. 39 (2011) 3049–3055. doi:10.1109/TPS.2011.2160209.

[12] X. Wang, W.T. Zheng, H.W. Tian, S.S. Yu, W. Xu, S.H. Meng, et al., Growth, structural, and magnetic properties of iron nitride thin films deposited by dc magnetron sputtering, Appl. Surf. Sci. 220 (2003) 30–39. doi:10.1016/S0169-4332(03)00752-9.

[13] L. C. Gontijo, R. Machado, E.J. Miola, L.C. Casteletti, P.A.P. Nascente, Characterization of plasma-nitrided iron by XRD, SEM and XPS, Surf. Coatings Technol. 183 (2004) 10–17. doi:10.1016/j.surfcoat.2003.06.026.

[14] E.J.D.M. Pillaca, M. Ueda, S. de F.M. Mariano, R. de Moraes Oliveira, Study of plasma immersion ion implantation inside a conducting tube using an E×B field configuration, Surf. Coatings Technol. 249 (2014) 104–108. doi:10.1016/j.surfcoat.2014.03.042.

[15] D.A. Shirley, High-Resolution X-ray Photoemission Spectrum of the Valance Bands of Gold, Phys. Rev. B. 5 (1972) 4709–4714.

[16] CasaXPS Manual 2.3.15 Rev 1.2. Introduction to XPS and AES. Neal Fairley. Casa Software Ltd. (2009).

[17] J.F. Moulder, W.F. Stickle, P.E. Sobol, K.D. Bomben, Handbook of X-ray Photoelectron Spectroscopy, 1992. doi:10.1002/sia.740030412.

[18] B. Vincent Crist, Handbooks of Monochromatic XPS Spectra, Volume 2 -Commercially Pure Binary Oxides, XPS International, LLC. 2 (2005) 1-172.

[19] B. Vincent Crist, Handbooks of Monochromatic XPS Spectra Volume 1 - The Elements and Native Oxides, Handb. Elem. Nativ. Oxides. 1 (1999) 1–43.

[20] P. Li, E.Y. Jiang, H.L. Bai, Fabrication of ultrathin epitaxial γ-Fe2O3 films by reactive sputtering, J. Phys. D. Appl. Phys. 44 (2011) 075003. doi:10.1088/0022-3727/44/7/075003.

[21] S. Chakravarty, N. Kumar, K. Panda, T.R. Ravindran, B.K. Panigrahi, S. Dash, et al., The influence of nitrogen concentration on microstructure and ultra-low friction behaviour of Fe-N thin films, Tribol. Int. 74 (2014) 62–71. doi:10.1016/j.triboint.2014.01.022.

[22] I. Bertóti, Characterization of nitride coatings by XPS, Surf. Coatings Technol. 151-152 (2002) 194–203. doi:10.1016/S0257-8972(01)01619-X.

[23] D.C. Kothari, M.R. Nair, A.A. Rangwala, K.B. Lal, P.M. Raole, xps studies at various temperatures steel of nitrogen 304 stainless, 8 (1985) 235–241. doi:075003075007.

[24] L. Shan, Y. Wang, J. Li, H. Li, X. Lu, J. Chen, Structure and mechanical properties of thick Cr/Cr2N/CrN multilayer coating deposited by multi-arc ion plating, Trans. Nonferrous Met. Soc. China. 25 (2015) 1135–1143. doi:10.1016/S1003-6326(15)63708-6.

[25] X. Tian, R.K.Y. Fu, L. Wang, P.K. Chu, Oxygen-induced nickel segregation in nitrogen plasma implanted AISI 304 stainless steel, Mater. Sci. Eng. A. 316 (2001) 200–204. doi:10.1016/S0921-5093(01)01245-X.

[26] M. Ueda, A.R. Silva, C.B. Mello, G. Silva, H. Reuther, V.S. Oliveira, Influence of the residual oxygen in the plasma immersion ion implantation (PI3) processing of materials, Nucl. Instruments Methods Phys. Res. Sect. B Beam Interact. with Mater. Atoms. 269 (2011) 3246–3250. doi:10.1016/j.nimb.2011.04.095.

ABOUT THE ORGANIZER

MARCOS AUGUSTO DE LIMA NOBRE: Assistant Professor and Researcher (2006 - present), with citation name M. A. L. Nobre, at the São Paulo State University (UNESP), School of Science and Technology, Department of Physics, campus at Presidente Prudente-SP. Head and Founder (2002) of the Laboratory of Functional Composites and Ceramics (LaCCeF acronym in Portuguese, the native idiom), Lab certified by PROPE-UNESP/National Council for Scientific and Technological Development/CNPq*. Grants from National Council for Scientific and Technological Development (CNPq), 2020-2023, 2019-2021 and 2010-2012. Granted with Young-Researcher scholarship by the São Paulo Research Foundation, FAPESP (São Paulo, São Paulo) (2002 - Summer of 2005). Postdoctoral fellow at the Polytechnic School of the University of Sao Paulo (POLI USP-SP) Metallurgy and Materials Science Department with FAPESP Scholarship (1999-summer of 2000). PhD in Science, CAPES Scholarship (Physical Chemistry 1999) by the Chemistry Department, UFSCar-SP. Master in Chemistry CNPq scholarship (Physical Chemistry 1995) by the Chemistry Department, UFSCar-SP. Licentiate degree (4-year of study) in Physics (1993) CNPq and CNPq-Rhae scholarships by the Physics Department, UFSCar-SP. Associate Editor of the Micro & Nano Letters - IET 2019-2020. Associate Editor of the Micro & Nano Letters-Wiley, 2020 - present. Ethycal Editor of the Applied Mathematics Science (Reuse) m-Hikari and Modern Research in Catalysis, Irvine-CA, USA (2017- date). Editorial board member of the Artemis Editora, Brazil. Nowadays, have 02 patents. Has published 80 papers at 39 different indexed Journals of renowned Editors. In May/25/2021, has been cited 1379 times, at 76 papers (47 with citations), in according to the ResearchID actual Publons base having an H-index equal to 23. Academic Google score: H = 28, i10 = 45 and 2338 citations. Reviewer of more than three dozen of journals. Have more than 580 communications and presentation in National and International Congress and Symposiums, from these 150 has been published as Conference Paper. Author or co-author of 20 Chapters of book approaching Scientific Divulgation, Teaching of Physic and Chemistry for teachers actuating in the graduating degree. For this, the Nanoscience and Nanotechnology have been the first strategy. Received tens of National and International Awards, Honorable mentions and distinction mentions, as well as titles. Research skills: Materials Science, Advanced Ceramic Processing, Linear and Non-linear Advanced Dielectrics Materials, Solid state chemistry, Impedance spectroscopy of solids and fluids, Structural Characterization via Mid infrared Spectroscopy with Fast-Fourier-Transformed of solid and fluids, Structural and non-structural Phase Transitions in Semiconductor Ferroelectrics. Also, Molecular Interactions in Functional Fluids as biofuels and its blends, probed via mid infrared Spectroscopy. Research interests: New Functional Materials as

amorphous composite based on carbon/nanoparticles and Semiconductor Ferroelectrics. Member of the Program of Post-Graduation in Chemistry at UNESP - Campus of São José do Rio Preto, IBILCE UNESP – SP, Brazil.

INDEX

G

K

M

N

O

Z

EDITORA
ARTEMIS